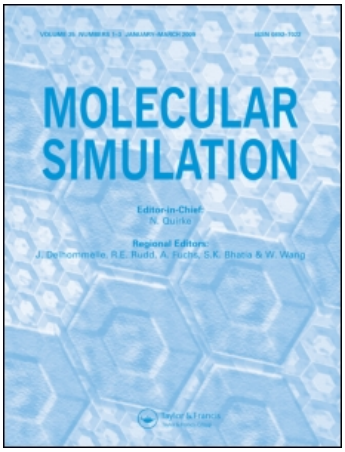

Molecular Simulation
Publication details, including instructions for authors and subscription information:
http://www.informaworld.com/smpp/title~content=t713644482

Stokesian Dynamics Simulations of Colloids Under Shear

P. J. Mitchell[a]; D. M. Heyes[a]
[a] Department of Chemistry, University of Surrey, Surrey, U.K.

To cite this Article Mitchell, P. J. and Heyes, D. M.(1995) 'Stokesian Dynamics Simulations of Colloids Under Shear', Molecular Simulation, 15: 6, 361 — 380
To link to this Article: DOI: 10.1080/08927029508022348
URL: http://dx.doi.org/10.1080/08927029508022348

Molecular Simulation, 1995, Vol. 15, pp. 361–380
Reprints available directly from the publisher
Photocopying permitted by license only

STOKESIAN DYNAMICS SIMULATIONS OF COLLOIDS UNDER SHEAR

P. J. MITCHELL and D. M. HEYES

Department of Chemistry, University of Surrey, Guildford, Surrey, GU2 5XH, U.K.

(Received May 1995, accepted May 1995)

Stokesian dynamics, SD, simulations of model colloidal dispersions under shear flow are presented. The behaviour of the Ermak Rouse-level model, which has no many-body hydrodynamics, MBH, is compared with the Ermak-McCammon algorithm which introduces MBH at the Rotne-Prager far-field level. Despite the inclusion of far field many-body hydrodynamics, the model colloidal systems still form ordered phases under shear very similar to those formed by the Rouse model, over what is now considered to be an unrealistically large part of the non-equilibrium shear rate vs. volume fraction phase diagram. There is even evidence that these many-body hydrodynamics promote the formation of ordered phases. We conclude that it is essential to have a better representation of short-range hydrodynamics (*e.g.* lubrication) forces in any realistic implementation of MBH in a SD simulation.

KEY WORDS: Stokesian dynamics, colloids, many-body hydrodynamics.

1 INTRODUCTION

In a previous publication [1] we calculated changes in the macroscopic properties of colloidal dispersions under shear flow (*e.g.* relative viscosity difference and structure factor) simulated by Rouse-level Brownian Dynamics, and compared these with changes in the microstructure of these dispersions. Here we investigate the effect of the introduction of a simple many-body hydrodynamics model into the simulations, using the Ermak-McCammon algorithm including the Rotne-Prager translational diffusion tensor.

Previous simulations using Rouse-level Brownian dynamics (BD) [1, 2], and molecular dynamics (MD) [3, 4], have shown the onset of order in dispersions with increasing shear rate. This order takes the form of lines or 'strings' of particles aligned along the flow direction of the shear, and pointing perpendicular to the vorticity and shear gradient plane. The formation of strings may be preceded by layering in the flow-vorticity plane, but there is some debate as to whether the layering is a real phase or just a transient structure. Some experimental observations using small angle neutron scattering (SANS) have also shown ordering of dispersions under shear, however, this ordering has been interpreted as the formation of strings of particles, but along the vorticity direction, *i.e.* perpendicular to the simulated strings [5]. The structure factors calculated for the simulated dispersions do, however, show a characteristic interparticle spacing in the flow direction (along the simulated 'strings'), which is consistent with the experimental interpretation of 'strings' along the vorticity direction regularly

spaced along the flow direction. The simulated 'strings' do not correlate longitudinally, and so order along the flow direction is not obvious from the real space configurations [1]. Rouse level Brownian Dynamics simulations show these ordered phases down to volume fractions at least as low as 0.3 and arbitrarily high shear rates. In contrast, most neutron and light scattering experiments do not indicate incipient ordering at these densities and shear rates. It is reasonable to assume that this discrepancy lies in the absence of realistic solvent-mediated forces in the model, so-called many-body hydrodynamics. In this study we include these interactions using a simple far-field expansion, described in the next section.

2 SIMULATION

The Rouse-level simulations carried out here were performed using the BD technique detailed in our previous work [1,2]. We introduced many-body hydrodynamic interactions using the configuration dependent Rotne-Prager translational diffusion tensor [6], which has been applied to equilibrium simulations [7, 8], and the simulation of flocs under shear conditions [9–11].

2.1 Brownian Dynamics

At the Rouse level the particle position update algorithm, based upon the Langevin equation of motion, is [12]:

$$\mathbf{r}_i(t+\delta t) = \mathbf{r}_i(t) + \delta t \frac{\mathbf{F}_i^P(t) + \mathbf{F}_i^B(t)}{m\beta} + \delta t \underline{\mathbf{E}} \mathbf{r}_i(t) \tag{1}$$

where $\mathbf{F}_i^P$ is the force on each particle due to the pairwise-additive interparticle interaction ϕ, $\mathbf{F}_i^B$ is a Gaussian random (Brownian) force on each particle, and $m\beta = 3\pi\sigma\eta_s$ is the friction coefficient of the suspending medium. $\underline{\mathbf{E}}$ is the strain rate tensor. The components of the Gaussian random forces have the following properties [13],

$$\langle \mathbf{F}_i \rangle_\alpha = 0 \tag{2a}$$

$$\langle \mathbf{F}_i^2 \rangle_\alpha = \frac{6\pi k_B T \sigma \eta_s}{\delta t} \tag{2b}$$

where η_s is the viscosity of the suspending medium, δt is the simulation time step, and $\alpha = x, y, z$. Therefore the components of the random displacements of the particles have the property,

$$\langle \mathbf{R}^2 \rangle_\alpha = 2D_0 \delta t \tag{3}$$

Our simulations were sheared using Lees-Edwards sliding periodic boundary conditions [14], with a homogeneous shear field in the x direction, in the xy plane. Therefore

the strain rate tensor was,

$$\underline{\mathbf{E}} = \begin{pmatrix} 0 & \dot{\gamma} & 0 \\ 0 & 0 & 0 \\ 0 & 0 & 0 \end{pmatrix} \tag{4}$$

where $\dot{\gamma}$ is the shear rate in particle units (*length* $= \sigma$ and *time* $= \sigma\,(m/\varepsilon)^{1/2}$). We measure the reduced shear rate of our simulations using the following definition of the Péclet number, which is defined as half that used by some other workers [15, 16],

$$Pe = \frac{\tau_r \dot{\gamma}}{2} \tag{5}$$

where $\tau_r = 3\pi\sigma^3\eta_s/4k_BT$ is the structural relaxation time. The interparticle potential used in all of our simulations was:

$$\phi_{ij} = \varepsilon\left(\frac{\sigma}{r_{ij}}\right)^{36} \tag{6}$$

Our simulations were carried out using a reduced system of units, so $m = 1$, $\sigma = 1$ and $\varepsilon = 1$, in Equations (1) and (6), and $k_BT = 1$ also.

2.2 *Many-Body Hydrodynamics*

Ansell and Dickinson *et al.* have derived and used a particle position update scheme [9–11], that extends that of Ermak and McCammon [7] from the equilibrium case into the shear flow regime. This scheme is based upon the particle configuration dependent translational diffusion tensor, typically represented by the Oseen or Rotne-Prager tensor forms.

$$\mathbf{r}_i(t+\delta t) = \mathbf{r}_i(t) + \frac{\delta t}{k_BT}\sum_{j=1}^{N} \underline{\mathbf{D}}_{ij}(t)\mathbf{F}_j(t) + \mathbf{R}_i(t,\delta t) + \underline{\mathbf{S}}_i(t)\underline{\mathbf{E}}\delta t + \dot{\gamma}(t)\delta t\underline{\mathbf{E}}\mathbf{r}_i(t) \tag{7}$$

where $\mathbf{r}$ is the particle position, $\underline{\mathbf{D}}$ is the diffusion tensor, $\mathbf{F}$ is the interparticle force, $\mathbf{R}$ is the random displacement and $\underline{\mathbf{S}}$ is the shear tensor.

The diffusion tensor used in these many-body hydrodynamics simulations was the Rotne-Prager tensor, for which the self terms are given by [6, 7],

$$\underline{\mathbf{D}}_{ii} = \frac{k_BT}{3\pi\eta_s\sigma}\underline{\mathbf{I}} \tag{8a}$$

and the interparticle terms by,

$$\underline{\mathbf{D}}_{ij} = \frac{k_BT}{8\pi\eta_s r_{ij}}\left[\left(\underline{\mathbf{I}} + \frac{\mathbf{r}_{ij}\mathbf{r}_{ij}}{r_{ij}^2}\right) + \frac{\sigma^2}{2r_{ij}^2}\left(\frac{1}{3}\underline{\mathbf{I}} - \frac{\mathbf{r}_{ij}\mathbf{r}_{ij}}{r_{ij}^2}\right)\right] \tag{8b}$$

where $\underline{\mathbf{I}}$ is the unit tensor. For a homogeneous shear field in the x direction, with the shear gradient in the y direction, the (third rank) shear tensor for each particle is given by,

$$\underline{\mathbf{S}}_i = \frac{5}{16}\sigma^3 \sum_{j \neq i} \frac{\mathbf{r}_{ij}\mathbf{r}_{ij}\mathbf{r}_{ij}}{r_{ij}^5} \tag{9}$$

Previous authors [9–11] have defined the strain rate tensor in its symmetrised, or pure shear, form.

$$\underline{\mathbf{E}} = \frac{1}{2}\begin{pmatrix} 0 & \dot{\gamma} & 0 \\ \dot{\gamma} & 0 & 0 \\ 0 & 0 & 0 \end{pmatrix} \tag{10}$$

However, this form is inconvenient for Rouse-level simulations (see the last term in Equation (1)). Also the product $\underline{\mathbf{S}}\underline{\mathbf{E}}$, which is a vector whose elements i are defined by,

$$\sum_j \sum_k S_{ijk} E_{kj} \tag{11}$$

is unaffected by the symmetrisation of $\underline{\mathbf{E}}$, because of the symmetry already present in $\underline{\mathbf{S}}$. Therefore, for clarity and ease of use, we adopte the non-symmetrised form of the strain rate tensor shown in Equation (4) for our simulations.

In Equation (7) the random (Brownian) displacements, $\mathbf{R}$, are not simply the Gaussian distribution of forces or displacements of Equations (1) and (3), because the diffusion coefficient in Equation (3) must be replaced by the diffusion tensor. As a result the mean square random displacements are given by,

$$\langle \mathbf{R}_i \mathbf{R}_j \rangle = \frac{6\mathbf{D}_{ij}}{\delta t} \tag{12}$$

which gives us a correlation of the random forces with the diffusion tensor. Equation (12) is asymptotic to Equation (3) as particle separation goes to infinity, because the diffusion tensor $\underline{\mathbf{D}}$ (Eq. (8)) becomes isotropic (i.e. $\underline{\mathbf{D}} = D_0\underline{\mathbf{I}}$). However, at short range the diffusion of each particle is no longer isotropic, but highly correlated. This gives rise to the second term on the right hand side of Equation (7). The correlation of the Brownian displacements is achieved by,

$$R_i(t, \delta t) = \sum_{j=1}^{i} L_{ij} X_j(t, \delta t) \tag{13}$$

where $\underline{\mathbf{L}}$ is the lower triangular 'square root' of the diffusion tensor $\underline{\mathbf{D}}$ (just as the RMS fluctuation of the uncorrelated random forces is the square root of Equation (3)); and $\mathbf{X}_j$ is the Gaussian random component for each particle, $\langle X_j^2 \rangle = 2/\delta t$. The 'square root'

(or Choleski decomposition) of the diffusion tensor is given by,

$$L_{ii} = \left(D_{ii} - \sum_{k=1}^{i-1} L_{ik}^2 \right)^{1/2} \tag{14a}$$

$$L_{ij} = \frac{1}{L_{jj}} \left(D_{ij} - \sum_{k=1}^{j-1} L_{ik} L_{jk} \right)^{1/2} \quad i > j \tag{14b}$$

The correlation arising from the interparticle interaction forces and the Brownian forces are of a fundamentally different form. The direct interparticle interaction forces are not affected by the nature of the suspending medium, whereas the Brownian forces arise from the medium itself.

Unfortunately for our computer simulations, the Rotne-Prager tensor is a $3N \times 3N$ matrix, and therefore so is $\underline{\mathbf{L}}$ (albeit lower triangular), which makes this part of the simulation extremely memory intensive and slow for the number of particles usually used in simulation (> 100). Equation (14) defines each element of $\underline{\mathbf{L}}$ as a loop over other elements, which means that the calculation of $\underline{\mathbf{L}}$ is effectively an N^3 problem. This limits us to simulations of small numbers of particles, and our simulations using this method have all been performed using $N = 32$. Further, Equation (8b) gives us isotropic terms of order $1/r_{ij}$, where r_{ij} is the interparticle centre-centre separation distance. These will have an effective range greater than the simulation box size for small systems. Untreated, this would give rise to large discontinuities in the diffusion tensor interactions at the cut-off radius, resulting in spurious dynamics. As a result we have smoothly reduced all the off-diagonal (interparticle) elements of the Rotne-Prager tensor by the factor $\exp(-r_{ij})$, which erodes the diffusion tensor to an insignificant value at typical cut-off separations. The Rotne-Prager tensor is diagonally dominant, and the off-diagonal terms are dominated by nearest neighbour contributions (*i.e.* those least affected by the truncation), so this approximation is perhaps not as serious as first might be considered.

2.3 *Relative Viscosity Differences*

The relative viscosity difference is the difference between the viscosity of the simulated system at the given shear rate, and the same system at infinite shear rate, *i.e.* the change in the viscosity of the system due only to the effect of shear upon the system. This is defined by:

$$\eta_{rd}(\dot{\gamma}) = \eta_r(\dot{\gamma}) - \eta_{r\infty} = \frac{\sigma_{xy}}{\dot{\gamma}\eta_s} \tag{15}$$

where σ_{xy} is the xy shear stress, and η_s the viscosity of the suspending medium. Our simulations assume a Newtonian and free-draining suspending medium, so effectively $\eta_{r\infty}$ is zero. Experimentally measured relative viscosity differences are often represented by:

$$\eta_{rd}(\dot{\gamma}) \sim Pe^{-\alpha} \tag{16}$$

where α is an adjustable parameter. In the shear rate regime between the first and second Newtonian plateaux (*i.e.* the shear thinning region) the simulated relative viscosity differences fit this form quite well.

Using log-log plots of simulated relative viscosity differences calculated according to Equation (15), a definite change of slope has been seen in Rouse-level simulations [1], which appears to be associated with the microstructural changes that occur in these systems with increasing shear rate (*e.g.* semi-order states leading up to the string phase).

2.4 *Structure Factors*

Structure factors can be calculated directly from particle configurations [17]:

$$S(\mathbf{k}) = \frac{1}{N}\left\langle \left(\sum_{j=1}^{N} \sin(\mathbf{r}_i \cdot \mathbf{k}) \right)^2 + \left(\sum_{j=1}^{N} \cos(\mathbf{r}_i \cdot \mathbf{k}) \right)^2 \right\rangle \tag{17}$$

where $\mathbf{r}$ is the position of each particle, and $\mathbf{k}$ is the reciprocal space vector, and the angled brackets ($\langle\ \rangle$) indicate a time average. For an unsheared system, the reciprocal vector is:

$$\mathbf{k} = \frac{2\pi}{L}\mathbf{n} \quad \text{where} \quad \mathbf{n} = \begin{pmatrix} n_x \\ n_y \\ n_z \end{pmatrix} \tag{18}$$

and L is the simulation cell side length. For sheared system this definition must be modified because the simulation cell is not the unit cell of the sheared periodic system [1]. The reciprocal vector becomes:

$$\mathbf{k} = 2\pi \begin{pmatrix} n_x/L_x \\ n_y/L_y - n_x \tan(\theta)/L_x \\ n_z/L_z \end{pmatrix} \tag{19}$$

where θ is the angle between the orthorhombic simulation cell and the sheared rhombohedral unit cell of the periodic system.

3 RESULTS

3.1 *Structures*

We have performed Rouse-level simulations on 256 particle systems over a range of volume fractions between 0.3 and 0.47. It is necessary to go to higher shear rates to form the string phase as volume fraction decreases. [1] (see Figs. 1 to 4 and Table 1). As the shear rate increases the strings become more fully established and straighter, showing no sign of disappearing or rearranging into a different ordered form.

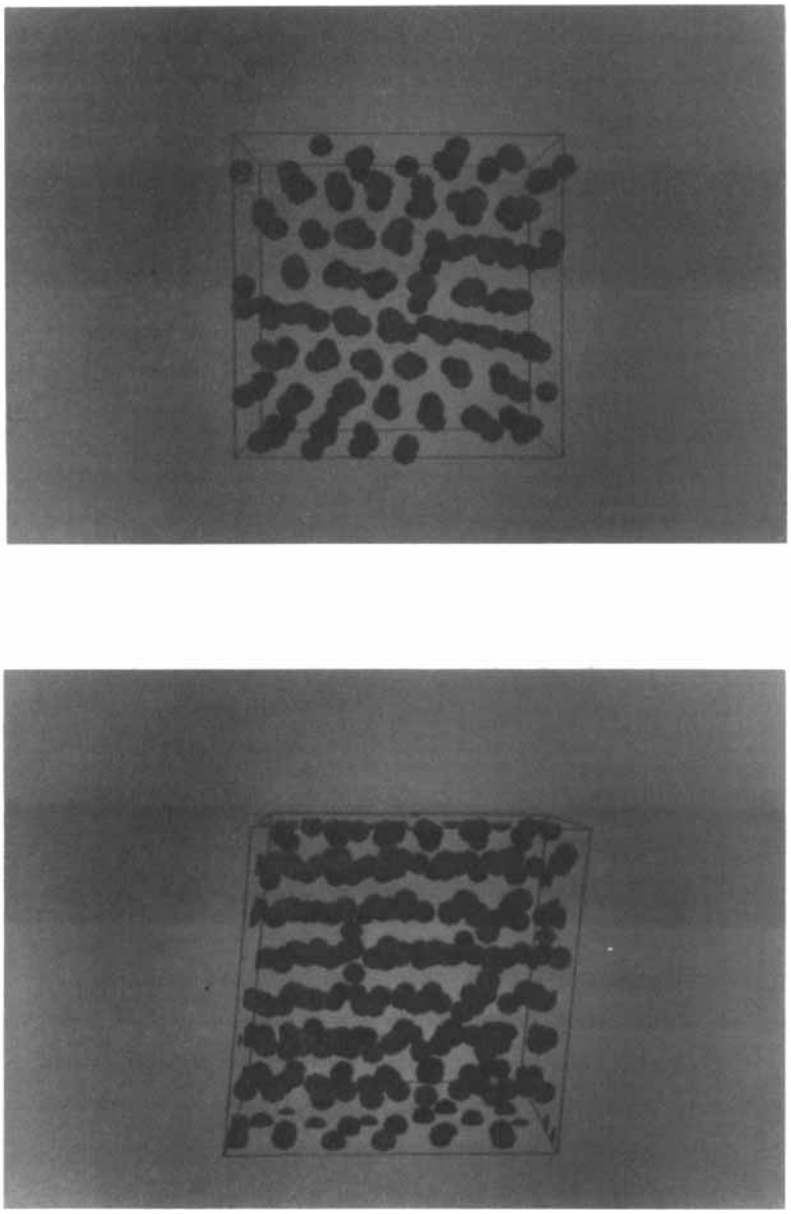

Figure 1 Particle configuration of a Rouse-level simulation of 256 particles at a volume fraction of 0.472, and a shear rate of 20 Péclet, viewed along a) the flow direction, and b) approximately the vorticity direction. Particle 'strings' occupy the whole systems at the given shear rates, and at all higher simulated shear rates. Particles shown at half diameter. See Color Plate I.

The many-body hydrodynamics simulations also show a fully established 'string' phase at similar shear rates to the Rouse-level simulations. It is not easy to anticipate what the effect of these changes to the equation of motion will be. The many-body coupling of the interaction and Brownian forces in our hydrodynamics simulations

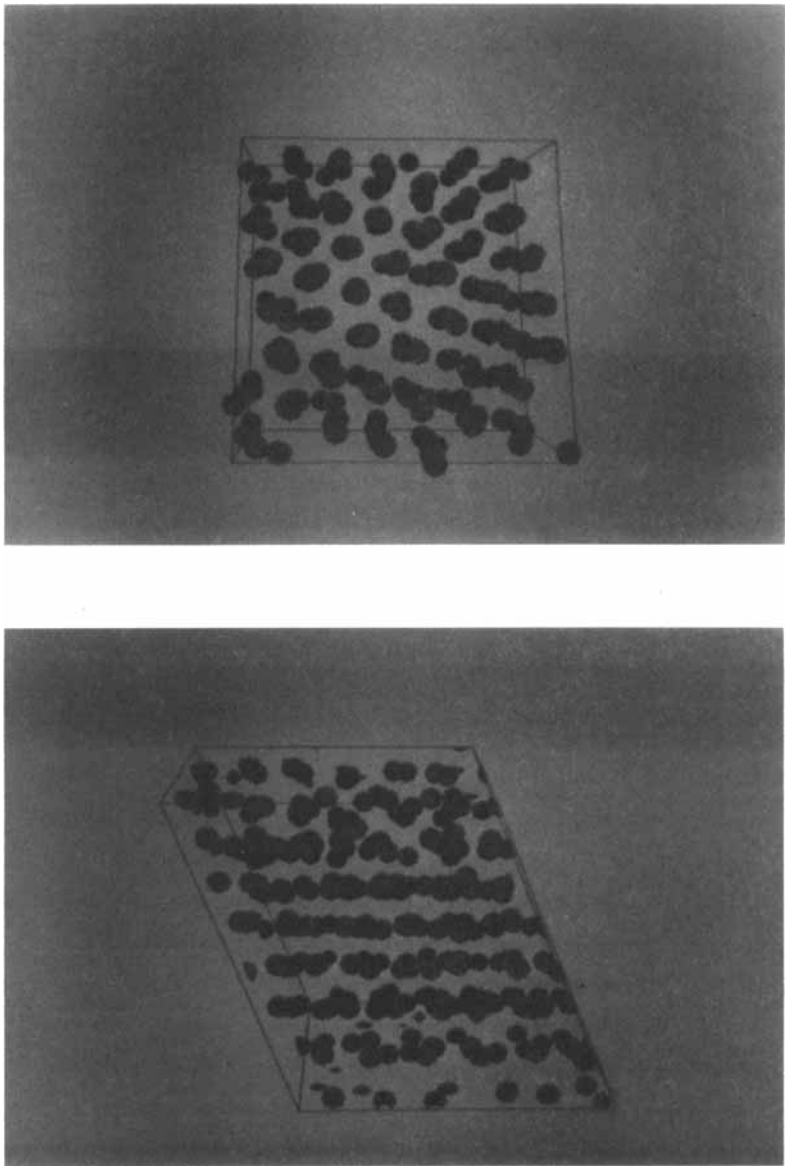

Figure 2 Particle configuration as Figure 1 but at a volume fraction of 0.45, and a shear rate of 25 Péclet. See Color Plate II.

could promote or hinder the formation of ordered structures. Examination of the particle configurations, particularly at low volume fractions, show that the hydrodynamics simulations appear to become ordered at lower shear rates than the Rouse-level simulations. Figure 5 shows the particle configurations, looking along the

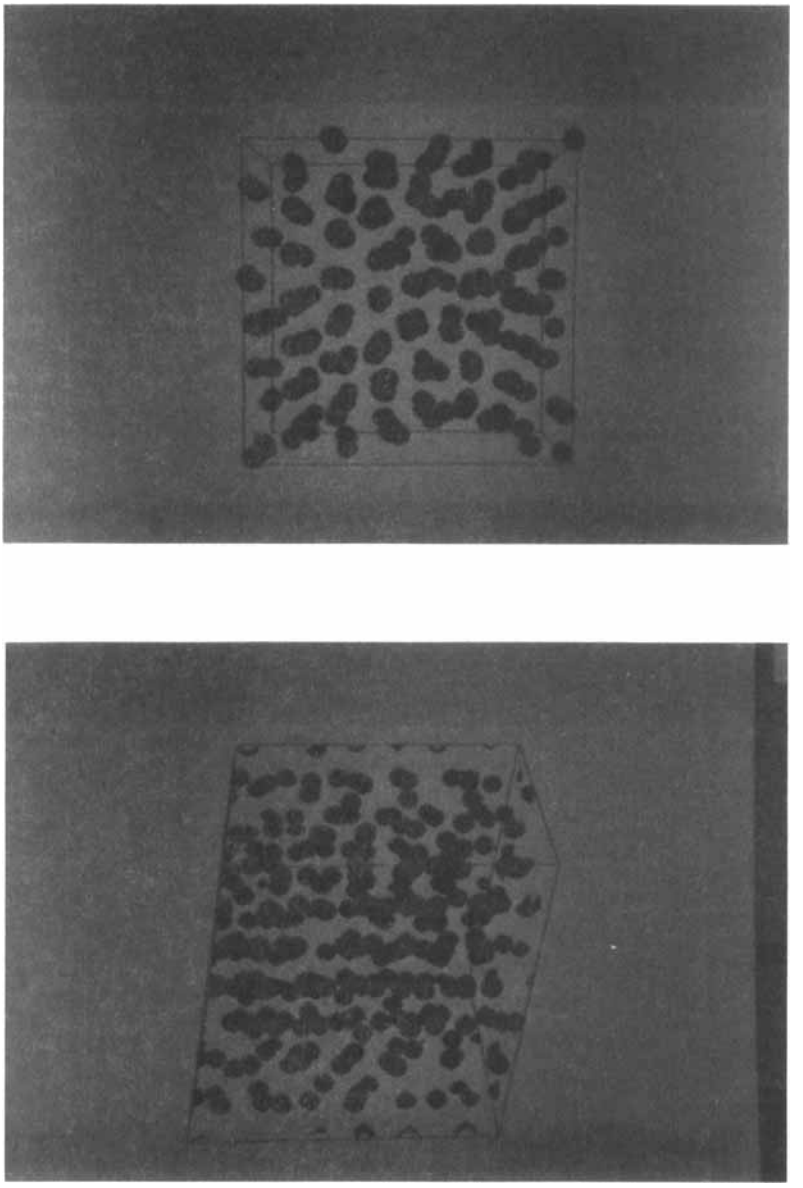

Figure 3 Particle configuration as Figure 1 but at a volume fraction of 0.40, and a shear rate of 50 Péclet. See Color Plate III.

flow direction, for 32 particle simulations at a volume fraction of 0.30, using the Rouse and many-body hydrodynamics models. The simulation cell's nearest neighbour periodic images are also shown to help establish any long range order with Figures 1 to 4. Although small system sizes generally enhance the amount of ordering within the

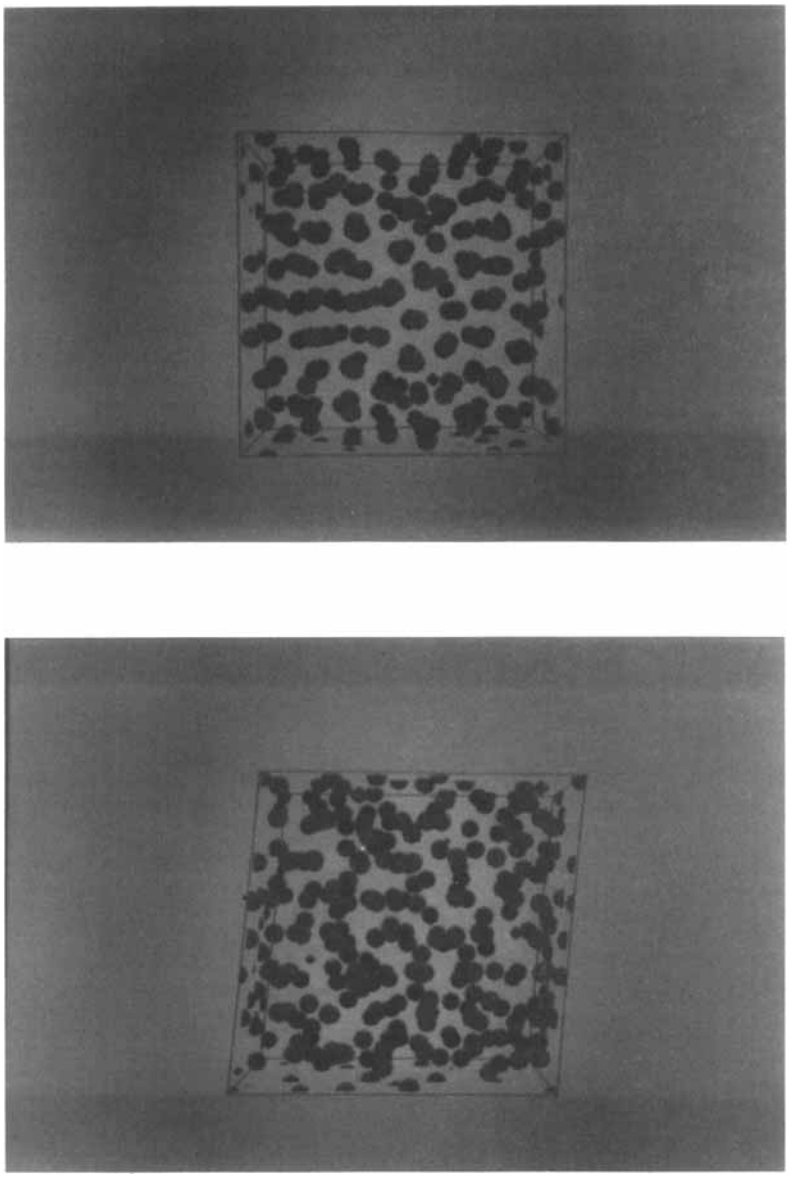

Figure 4 Particle configurations as Figure 1 but at a volume fraction of 0.30, and a shear rate of 100 Péclet. See Color Plate IV.

systems, above that seen in larger systems (Figs. 1 and 4), the small hydrodynamics simulations shown in Figure 5 show more evidence of ordering in the form of layers and strings than the small Rouse-level simulation also shown in this figure. This enhanced ordering can only be due to the correlated nature of the forces on the particles embodied in Equation (7) leading to correlation of particle positions.

Table 1 The approximate shear rate at which the 'string' phase is fully established in our Rouse-Level BD simulations, at a range of volume fractions.

ϕ	Pe
0.472	20
0.45	25
0.40	50
0.30	100

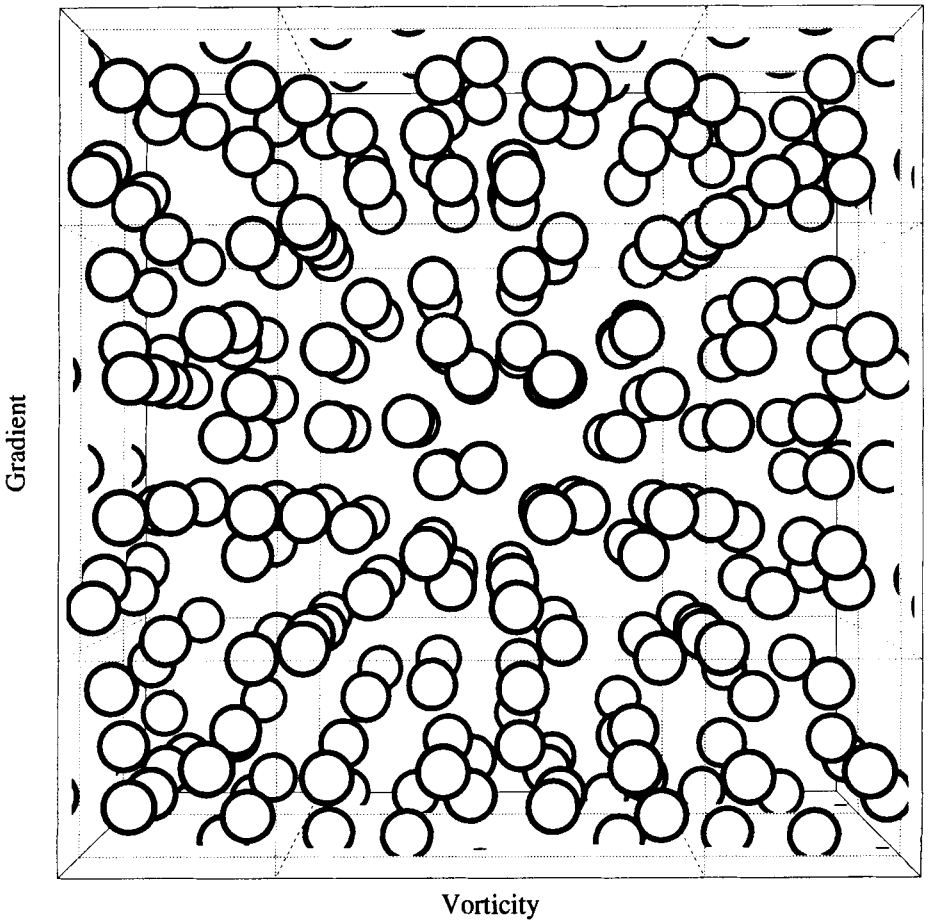

Figure 5 The particle configurations viewed along the flow direction for a) Rouse-level and b) many-body hydrodynamics simulations of 32 particles at a volume fraction of 0.30. The periodic images of the particles are also shown. There appears to be more ordering in the hydrodynamics simulation than in the Rouse-level simulation. Particles shown at half diameter.

N:	32
Volume Fraction:	0.300
Peclet Number:	10.000
Total Strain:	716.217
Age:	8895.183

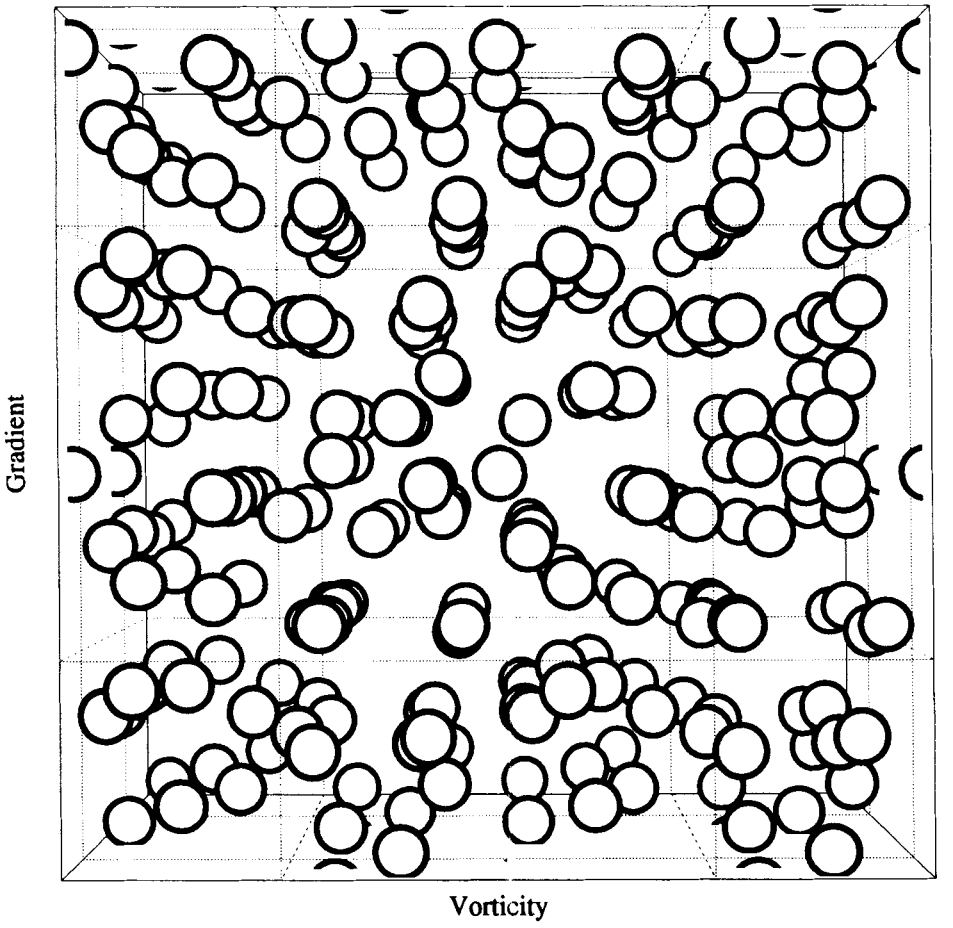

Figure 5 *(Continued).*

3.2 Relative Viscosity Differences

In Figure 6 we see the relative viscosity differences for 32 particle simulations both with, and without, many-body hydrodynamics. Careful examination of these figures reveals a change of slope, on the log-log scale, which is associated with incipient long range order. At higher shear rates this develops into the string phase. In the Rouse-level

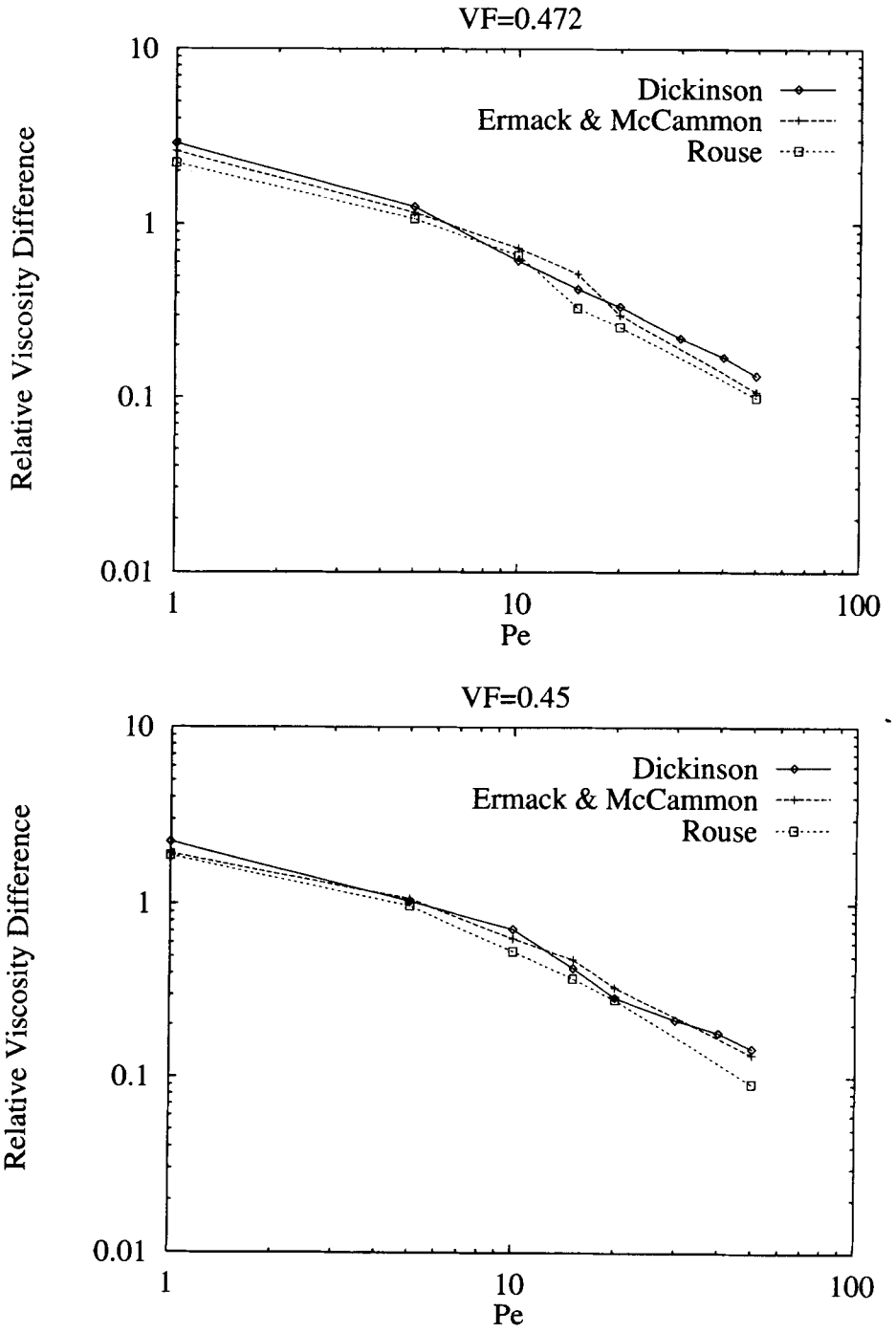

Figure 6 The relative viscosity differences, on a log-log plot, for simulated systems of 32 particles at the volume fractions of a) 0.472, b) 0.45, c) 0.40 and d) 0.30. The three simulation models (Rouse, Ermak & McCammon and Ansell & Dickinson) are shown for each density. There is a change in the power-law dependence of the relative viscosity difference for the first two models, and no apparent change for the third.

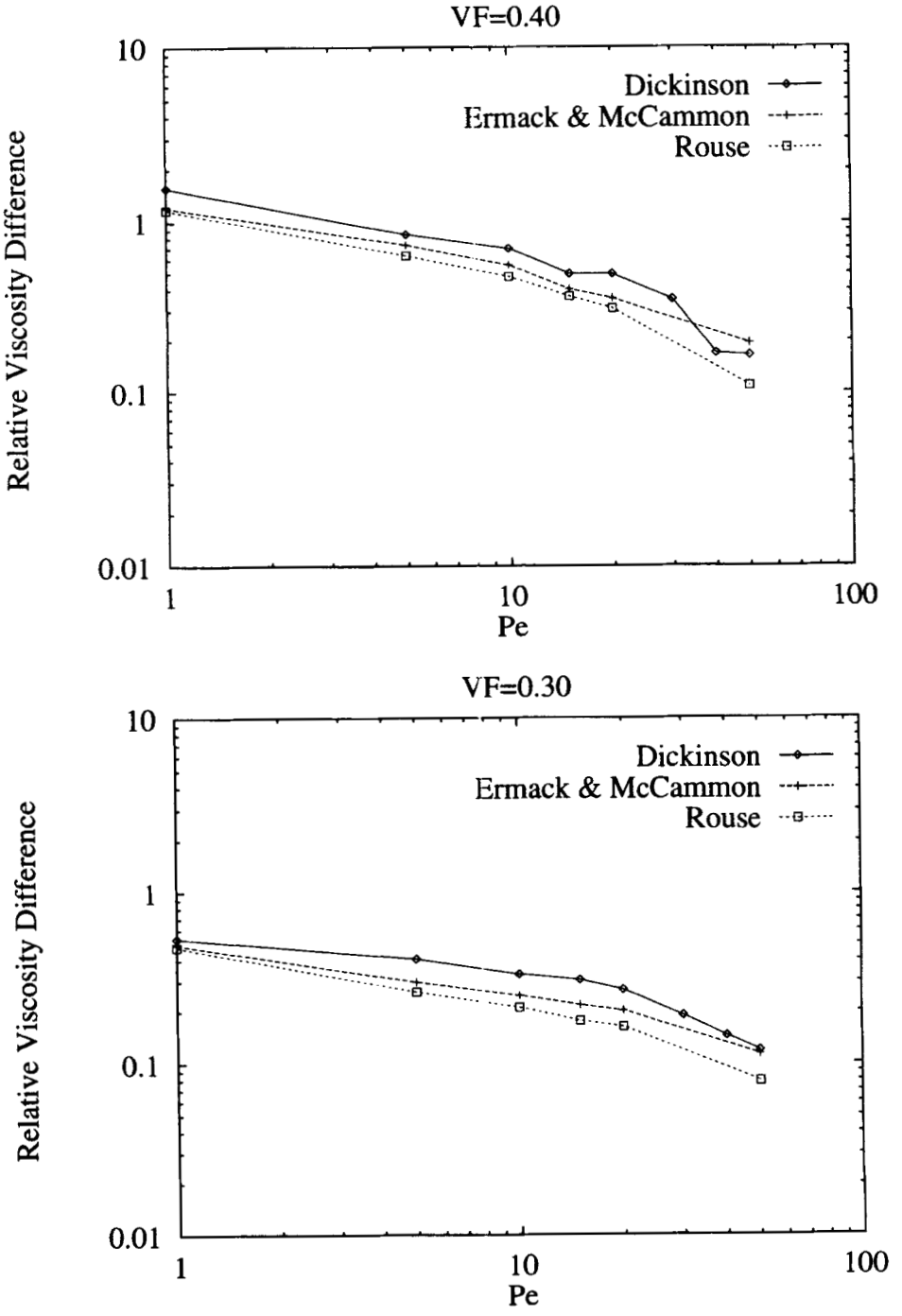

Figure 6 *(Continued).*

simulations the change of slope of the lines occurs at higher shear rates for lower volume fractions. This is in accordance with the observed delay in ordering to higher shear rates as volume fraction decreases. The change of slope becomes less sharp with decreasing density, and at a volume fraction of 0.30 it is difficult to see a particular transition point. It should be noted that although some 'strings' of particles are present at the 'knee' point of the lines in Figure 6, there are significant numbers of particles still in layered or amorphous structures. The 'string' phase is not fully established until higher shear rates.

The many-body hydrodynamics simulations show similar behaviour to the Rouse-level simulations, with a change of slope occurring at statistically the same shear rate values. However, they do show a fairly consistent enhancement of the relative viscosity difference at all shear rates. This indicates, perhaps, that the coupling of forces in the many-body hydrodynamics simulations makes any transient disordered local structures formed in the colloidal liquid under shear, slightly more long-lived, hence producing larger stresses under the influence of shear flow. For comparison we also show many-body hydrodynamics simulations using only the Ermak and McCammon algorithm (*i.e.* Eq. (7) without the last, shear/strain, term). The viscosities of these simulations lie between the Rouse-level and Dickinson model hydrodynamics simulation values. The Dickinson model has an explicit shear strain tensor term, not present in the Ermak & McCammon algorithm. Therefore the Dickinson model is a more complete description of the many-body hydrodynamics. It can be seen from Figure 6 the apparent difference in relative viscosity difference, between the Rouse-level and many-body hydrodynamics simulations, is a greater fraction at lower volume fractions. The far field hydrodynamics are more important at lower volume fraction, so it is consistent with our results that the viscosity should be most sensitive to the presence of many-body hydrodynamics at low volume fractions.

3.3 Structure Factors

Figures 7 and 8 show the directly calculated structure factors (Eq. (17)) for our Rouse-level simulations of 256 particles, at various volume fractions. Our calculated data are shown as points, and cubic splines are fitted to them to give some idea of their overall shape. Figure 7 shows that the peak along the flow axis in the Debye-Scherrer ring changes in position and intensity as shear rate is increased from zero. At high density ($\phi = 0.472$) the peak initially remains in the same place, but decreases in intensity. At higher shear rates however, the peak's intensity increases again, and it's position moves to lower k-vector. The movement to lower k-vector implies that the particles are moving farther apart along the flow direction, as expected. Also the peaks appear to be in two distinct groups, with the lower shear rate peaks being closer to each other than to the high shear rate peaks. This is indicative of the ordered phase that our Rouse-level simulations enter at high shear rates, with a structure much different to that at low shear rates or at rest. At lower densities ($\phi = 0.45, 0.40, 0.30$) the changes in the structure factor peak position and intensity are more gradual (as seen for the 0.30 example), which is consistent with the more gradual changes in the relative viscosity difference and observed ordering in real space.

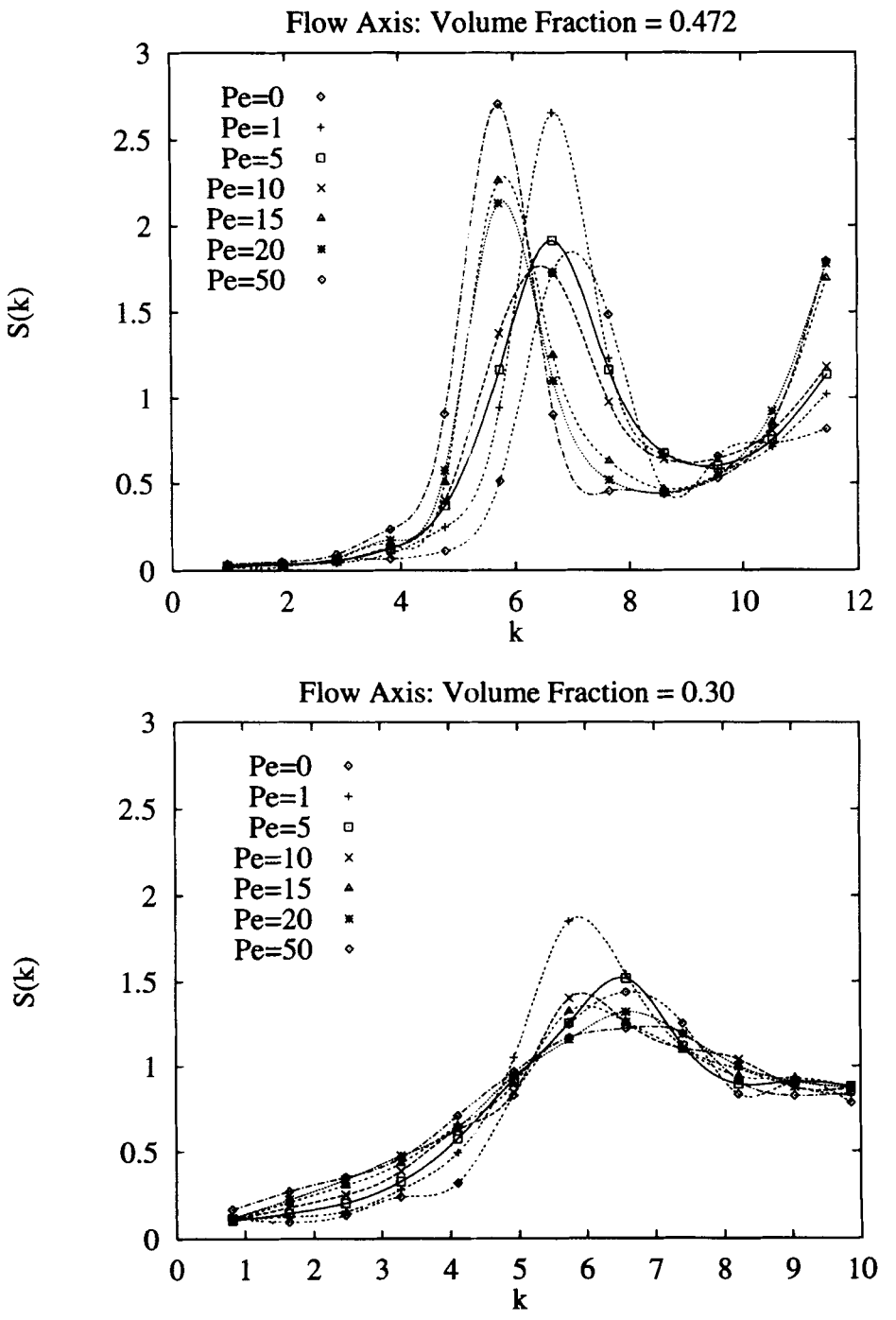

Figure 7 The directly calculated struture factors along the flow direction for Rouse-level simulations of 256 particles at volume fractions of a) 0.472 and b) 0.30. At high density the first peak moves to lower k-vector. The changes are less distinct at lower densities. The lines fitted to the data points are cubic splines.

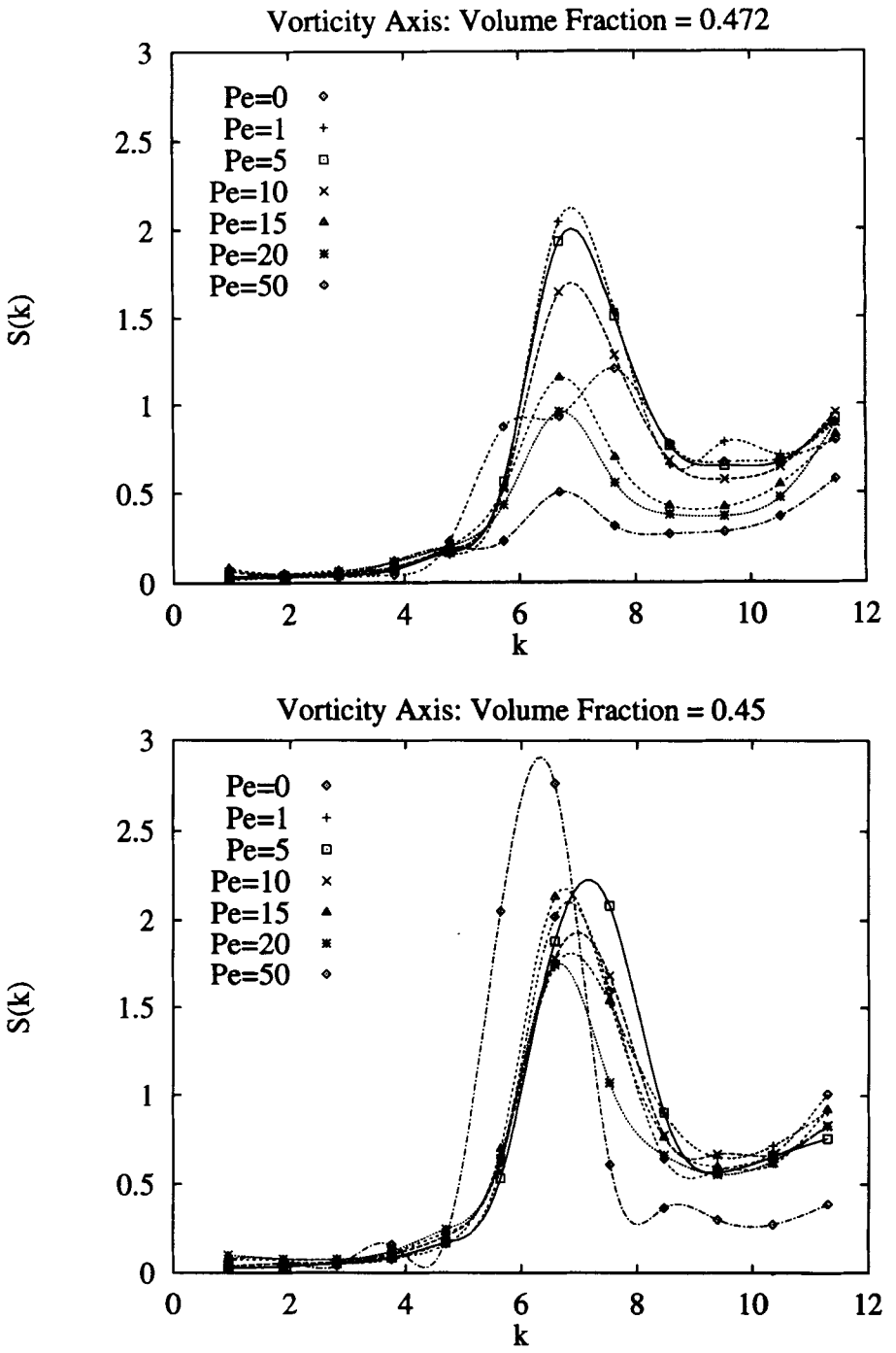

Figure 8 The directly calculated structure factors along the vorticity direction for Rouse-level simulations of 256 particles at volume fractions of a) 0.472, b) 0.45 and c) 0.30. At high density the first peak moves to lower k-vector. The changes are less distinct at lower densities. The lines fitted to the data points are cubic splines.

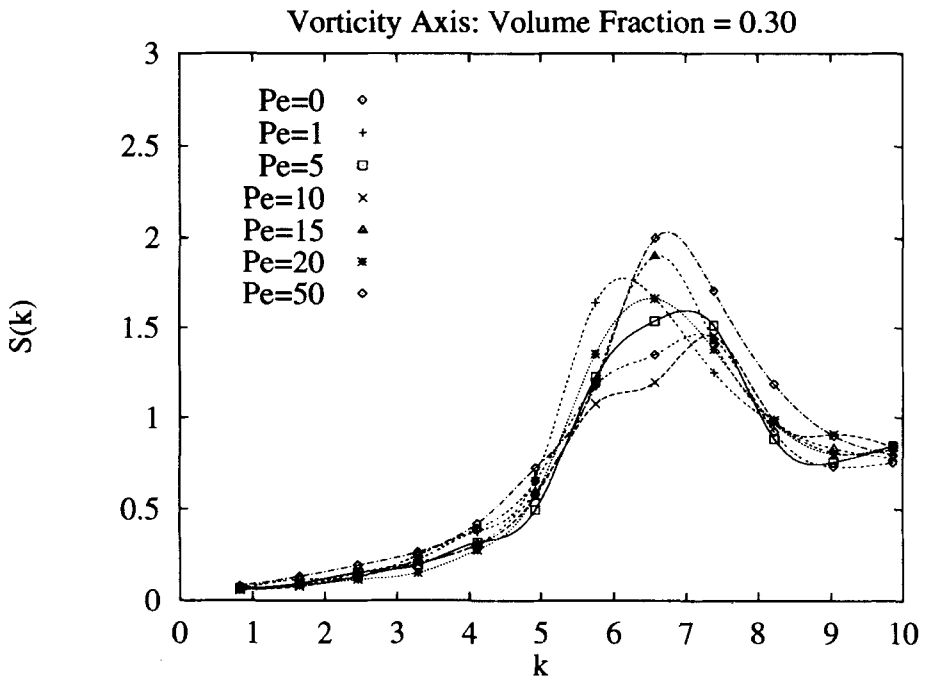

Figure 8 *(Continued).*

The behaviour of the structure factor along the vorticity direction (perpendicular to the shear plane) as a function of shear rate is, in many respects, quite different from along the flow direction. Figure 8 shows that, at the highest density, the Debye-Scherrer peak along the vorticity axis decreases in intensity with shear rate, but does not appear to move significantly. At the slightly lower density of $\phi = 0.45$ there is little change in intensity (except at the highest shear rate), but there is an apparent shift to higher k-vector. At lower densities the trends are less pronounced.

4 CONCLUSIONS

The states formed by the many-body hydrodynamics simulations differ only slightly from the Rouse-level simulations, despite the correlated nature of both the interparticle interaction and random Brownian forces in the many-body hydrodynamics model. Both the relative viscosity difference and structure factor data show very similar trends. Our calculated structure factors also show several qualitative agreements in trends (especially of the Debye-Scherrer peak) with experimental data [1]. The introduction of many-body hydrodynamics leads to a (small) enhancement of relative viscosity difference over Rouse-level simulations, and the transition at slightly lower shear rates to structures associated with high shear rates in the Rouse-level simulations. This difference becomes more pronounced as density decreases. This indicates that the

coupled nature of the forces in the many-body hydrodynamics simulations is leading to a slower relaxation of microstructural fluctuations under shear, especially at low density. The fluid therefore presents a greater resistance to the imposed flow.

These results are consistent with the view that far-field hydrodynamics is more important at low volume fraction, whereas at high volume fractions excluded volume and short range effects are probably of a greater importance [18]. The many-body hydrodynamics schemes used here are of a far-field nature. The Rotne-Prager and Oseen tensors are derived from the hydrodynamics of pairs of particles moving in a fluid which is at rest at infinity. We see from the relative viscosity difference data that the effect of the inclusion of many-body hydrodynamics is greater at lowest density. It would seem, then, that for simulations of dense suspensions the addition of near field many-body hydrodynamics effects are essential.

Acknowledgements

PJM thanks the EPSRC (Engineering and Physical Sciences Research Council) and ECC International Ltd. (English China Clays) for the award of a research fellowship.

References

[1] P. J. Mitchell, D. M. Heyes and J. R. Melrose, "Brownian dynamics simulations and light scattering studies of model stabilised colloidal dispersions under shear", *Faraday Transactions*, **91**(13), 1975–1989 (1995).

[2] D. M. Heyes and J. R. Melrose, "Brownian dynamics simulations of model hard-sphere suspensions", *J. Non-Newtonian Fluid Mech.*, **46**, 1–28 (1993).

[3] S. Nosé and M. L. Klein, "Constant pressure molecular dynamics for molecular systems", *Mol. Phys.*, **50**(5), 1055–1076 (1983).

[4] J. J. Erpenbeck, "Shear viscosity of the hard sphere fluid via nonequilibrium molecular dynamics", *Phys. Rev. Lett.*, **52**(15), 1333–1335 (1984).

[5] P. Lindner, I. Marković, R. C. Oberthür, R. H. Otterwill and A. R. Rennie, "Small angle neutron scattering studies of polymer latices", *Progr. Colloid Polym. Sci.*, **76**, 47–50 (1988).

[6] J. Rotne and S. Prager, "Variational treatment of hydrodynamic interaction in polymers", *J. Chem. Phys.*, **50**(11), 4831–4837 (1969).

[7] D. L. Ermak and J. A. McCammon, "Brownian dynamics with hydrodynamic interactions", *J. Chem. Phys.*, **69**(4), 1352–1360 (1978).

[8] G. K. Batchelor and J. T. Green, "The hydrodynamic interaction of two small freely-moving spheres in a linear flow field", *J. Fluid. Mech.*, **56**, 375–400 (1972).

[9] G. C. Ansell, E. Dickinson and M. Ludvigsen, "Brownian dynamics of colloidal-aggregate rotation and dissociation in shear flow", *J. Chem. Soc., Faraday Trans. 2*, **81**, 1269–1284 (1985).

[10] G. C. Ansell and E. Dickinson, "Brownian dynamics simulation of the fragmentation of a large colloidal floc in simple shear-flow", *J. Colloid Interface Sci.*, **110**, 73–81 (1986).

[11] M. C. Buján-Núñez and E. Dickinson, "Brownian dynamics simulation of a multi-subunit deformable particle in a simple shear flow", *J. Chem. Soc. Faraday Trans.*, **90**(18), 2737–2742 (1994).

[12] D. L. Ermak, "A computer simulation of charged particles in solution I & II", *J. Chem. Phys.*, **64**(10), 4189–4203 (1975).

[13] D. M. Heyes, "Rheology of molecular liquids and concentrated suspensions by microscopic dynamical simulations", *J. Non-Newtonian Fluid Mech.*, **27**, 47–85 (1988).

[14] A. W. Lees and S. F. Edwards, "The computer study of transport processes under extreme conditions", *J. Phys. C*, **5**, 1921 (1972).

[15] D. J. Evans, S. T. Cui, H. J. M. Hanley and C. G. Straty, "Conditions for the existance of reentrant solid phase in a sheared atomic fluid", *Phys. Rev. A*, **46**(10), 6731–6734 (1992).

[16] S. J. Johnson, C. G. de Kruif and R. P. May, "Structure factor distortion for hard-sphere dispersions subjected to weak shear flow: small-angle neutron scattering in the flow-vorticity plane", *J. Chem. Phys.*, **89**(9), 5909–5921 (1988).

[17] O. Hess, W. Loose, T. Weider and S. Hess, "Shear-induced anisotropy of the structure of dense fluids", *Physica B*, **156 & 157**, 505–507 (1989).

[18] B. H. A. A. van den Brule and R. J. J. Jongschaap, "Modeling of concentrated suspensions", *J. Stat. Phys.*, **62**(5/6), 1225–1237 (1991).